



Prediction of slowdown of the Atlantic Meridional Overturning Circulation in coupled model simulations

Kuniko Yamazaki¹ · Laura C. Jackson¹ · David M. H. Sexton¹

Received: 12 July 2023 / Accepted: 12 February 2024
© Crown 2024

Abstract

In coupled perturbed parameter ensemble (PPE) experiments or for development of a single coupled global climate model (GCM) in general, models can exhibit a slowdown in the Atlantic Meridional Overturning Circulation (AMOC) that can result in unrealistically reduced transport of heat and other tracers. Here we propose a method that researchers running PPE experiments can apply to their own PPE to diagnose what controls the AMOC strength in their model and make predictions thereof. As an example, using data from a 25-member coupled PPE experiment performed with HadGEM3-GC3.05, we found four predictors based on surface heat and freshwater fluxes in four critical regions from the initial decade of the spinup phase that could accurately predict the AMOC transport in the later stage of the experiment. The method, to our knowledge, is novel in that it separates the effects of the drivers of AMOC change from the effects of the changed AMOC. The identified drivers are shown to be physically credible in that the PPE members exhibiting AMOC weakening possess some combination of the following characteristics: warmer ocean in the North Atlantic Subpolar Gyre, fresher Arctic and Tropical North Atlantic Oceans and larger runoff from the Amazon and Orinoco Rivers. These characteristics were further traced to regional responses in atmosphere-only experiments. This study suggests promising potential for early stopping rules for parameter perturbations that could end up with an unrealistically weak AMOC, saving valuable computational resources. Some of the four drivers are likely to be relevant to other climate models so this study is of interest to model developers who do not have a PPE.

Keywords Atlantic Meridional Overturning Circulation (AMOC) · AMOC slowdown · Perturbed parameter ensemble (PPE) · Global climate model (GCM) development · Statistical methods · Amazon River

1 Introduction

The Atlantic Meridional Overturning Circulation (AMOC) is a major contributor to poleward heat transport and plays an important role in projections of regional climate (such as over Europe, e.g. Jackson et al. 2015). Recent RAPID observations (Moat et al. 2022), which are measured at 26°N, suggest decadal mean (calculated using a decadal sliding window over annual data over December 2004 to November 2019) mass transport of 16 Sv. If a coupled model underestimates the strength of the AMOC, it can cause the northern hemisphere in the model, particularly over land, to cool excessively. It also reduces the credibility of regional climate

projections. In model development, finding out whether the simulated AMOC will be too weak comes late in the process. Certainly in the development of the Met Office HadGEM3 series of models (e.g. Walters et al. 2019 and Williams et al. 2018), testing of multiple candidates is initially based on faster, more affordable atmosphere-only configurations, and coupling to an ocean model happens once the atmosphere-only model has been (almost) finalised. The next stage involves spinning up the coupled system from an initial state based partly on ocean reanalysis. Due to the slow time scales over which the AMOC evolves, it can take several decades of computer simulation to reveal if its strength is credible and useful.

The situation is even worse when generating a perturbed parameter ensemble (PPE) of coupled climate simulations such as the one developed for UK Climate Projections in 2018 (UKCP18; Murphy et al. 2018; Yamazaki et al. 2021). A PPE comprises multiple model variants, each with slightly

✉ Kuniko Yamazaki
kuniko.yamazaki@metoffice.gov.uk

¹ Met Office Hadley Centre, FitzRoy Road, Exeter EX1 3PB, UK

differently modified values of parameters representing key sub-grid-scale physical processes (e.g. Murphy et al. 2004; Stainforth et al. 2005; Sanderson 2011; Shiogama et al. 2012; Rowlands et al. 2012; Sexton et al. 2021; Yamazaki et al. 2021). It is prohibitively expensive in terms of time and computer resources to identify plausible parameter combinations using the full coupled model. Instead, we adopt an approach based on the one used in development of the single, tuned model. That is, a limited number of these combinations are selected using a relatively cheap version of the global climate model (GCM) (usually using only the atmosphere and land components, coarser grid resolution and shorter simulation time), and subsequently assigned to the fully coupled PPE (Karmalkar et al. 2019; Sexton et al. 2021).

In UKCP18 coupled PPE, 8 of the 25 members exhibited very low (values at or below 8 Sv by 1950) AMOC transport compared with CMIP5 models, excessive northern hemisphere cooling or excessive cold bias over Europe during the historical experiment, the latter of which is also associated with the unrealistically weak modelled AMOC (Yamazaki et al. 2021). The characteristics rendered these members unusable for making future projections. Thus, expensive computing resources were wasted, as well as resulting in a reduction in ensemble size (Murphy et al. 2018; Yamazaki et al. 2021) which then limits the potential uses of the PPE itself.

The reason this parameter selection method was ineffective in eliminating the AMOC-weakening perturbed parameter combinations was because the AMOC is an atmosphere–ocean coupled phenomenon; at the time we did not know how an atmosphere-land-only PPE could be used to predict the AMOC. Therefore, we need to devise a complementary approach to predict the AMOC weakening within the perturbed parameter combination selection process or at least in the early stage of the coupled PPE experiment.

We are not alone in facing the issue of the AMOC weakening upon coupling of model components. For example, a white paper from an international workshop on Earth System Processes describes outstanding issues as follows: “The workshop also discussed some of the challenges. Examples were highlighted, from the atmospheric chemistry, physical ocean and land surface/carbon cycle communities, of where the behaviour in fully coupled configurations can act in different directions to the simulations in offline or uncoupled experiments. ... examples were highlighted (of) different coupled vs offline behaviour in ... ocean modelling (magnitude of simulated AMOC)” (Booth, 2017, White Paper: Earth System Processes and Informing future UK Climate Projections, drawing on the July 2017 workshop Informing future UK climate projections, held in Exeter, UK., unpublished report). In response to this need, in this paper we address two ambitious questions:

Can we propose a generic method, which exploits simulated data from the spinup experiment of a coupled PPE to diagnose what controls the strength of the AMOC in the PPE and make predictions thereof, and which can be employed by other groups running PPE experiments? Can we demonstrate how this method works and how the results of the statistical methods can be physically substantiated, by using the UKCP18 HadGEM3-GC3.05 coupled PPE as an example?

The goal of using this method on a PPE is to uncover the processes that control the strength of the AMOC or to predict its value is to improve the design of that PPE. For instance, this method is a valuable approach for not wasting resources on members where the AMOC will weaken too much. Any specific numbers or regions or features derived as a result of applying the method to the UKCP18 HadGEM3-GC3.05 coupled PPE dataset and presented in this paper are examples and are not intended to be taken as something expected to be exactly the same across all other PPEs. Each different PPE will produce its own set of drivers, some of which might be similar to those from our PPE. In Sect. 4, we describe the mechanisms of the predictors to show that they, and therefore predictions based on them, are physically credible and that some of them are potentially relevant to other PPEs and climate models. Our results are therefore potentially useful for model developers whether they have a PPE or not and we discuss this in Sect. 5.

In applying the method to the HadGEM3-GC3.05 PPE, we exploit the data derived in the course of making UKCP18 land projections (Yamazaki et al. 2021; Sexton et al. 2021). We want a more reasonable AMOC strength at the end of the historical period where we have direct observations at 26 N (Moat et al. 2022). We find that the PPE members in which the AMOC weakened excessively during the historical phase (experimental phases will be described in the next section) generally showed reduced AMOC transport at 26 N at the end of the preceding spinup phase. Hence, in this study, we use the AMOC transport at 26 N averaged over the final 20 years of the spinup phase of the UKCP18 coupled PPE experiment to represent the AMOC strength in each ensemble member as the target for the prediction. Using the spinup phase, which is run under constant external forcing with seasonal cycle, has the benefit of both capturing the initial transient response of the models to parameter perturbations and aiding a cleaner analysis by avoiding the need to separate out the complex evolution of the climate state imposed by transient historical external forcing.

This paper is laid out as follows. In the next section, we describe the model and experimental design that were used in the production of the archived data used in this study. The methodology to diagnose the controlling factors of the strength of the AMOC and to predict it is presented in

Sect. 3. The mechanism of AMOC weakening that underpins the prediction methodology is shown in Sect. 4 and provides confidence that even if a PPE is not available, the key mechanisms might be relevant to the development of single, tuned climate models as well. We discuss this and summarise in Sect. 5.

2 Model and experimental design of the coupled PPE, AMOC behaviour in the coupled PPE and analysis methods used in this study

2.1 Model used in the coupled PPE experiment

We use archived data derived in the coupled PPE experiments (hereafter referred to as “COUPLED”) performed to make the UKCP18 land projections (Yamazaki et al. 2021; Sexton et al. 2021). The underlying model of the PPE is the Unified Model HadGEM3-GC3.05 coupled atmosphere–ocean–sea ice–land GCM, which is close to the GC3.1 version submitted to CMIP6 (Williams et al. 2018). For the atmosphere (Walters et al. 2019) and land (the Joint UK Land Environment Simulator (JULES) land surface model; Best et al. 2011; Clark et al. 2011) components of the model, we used the N216 resolution, which is 60 km in mid-latitudes. The atmosphere component has 85 levels in the vertical in non-equidistant hybrid height coordinates that follow the terrain at the surface. The top 30 levels represent the stratosphere and above, with a fixed lid at 85 km.

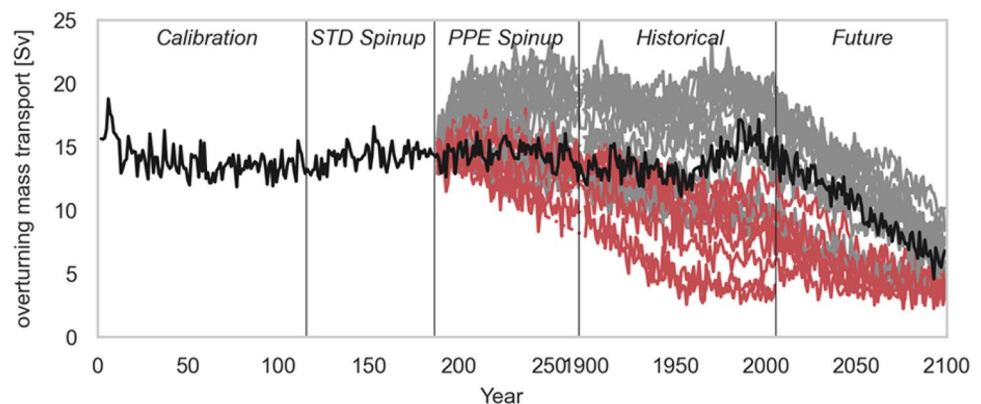
The land component represents land surface and sub-surface soil processes and employs the following: tiles to represent 9 sub-grid-scale vegetation and surface types, vegetation canopy approach, 4-layer scheme for soil processes, multi-layer snow scheme and river-routing scheme using the TRIP model (Oki and Sud, 1988) to calculate river-routing. The freshwater outflow from land to the ocean resulting from the river-routing scheme forms “an important component of the thermohaline circulation” (Walters et al. 2019).

The ocean component is NEMO (Madec et al. 2017; Hewitt et al. 2011) and has tripolar grid in the horizontal. We used the ORCA025 configuration in the global coupled PPE experiments for UKCP18 land projections, which has its coarsest resolution of 0.25 degrees in the vicinity of the equator. There are 75 levels in the vertical and the level thickness is smaller near the surface (Madec et al. 2017). We used the free-surface variable volume scheme, in which the volume (i.e. freshwater) flux (and the damping freshwater flux for flux adjustment if it is chosen) is distributed among all vertical levels in the same grid proportionately to their thickness. On the other hand, the salt flux from the sea ice (and the damping salt flux for flux adjustment if it is chosen) is added entirely to the surface level. The sea-ice model is CICE (Hunke and Lipscomb 2008; Hewitt et al. 2011), in which sea ice is modelled in 4 layers and topped with 1 layer of snow. CICE includes dynamics as well as thermodynamics of sea-ice processes and exchanges heat, freshwater and momentum with both the atmosphere and ocean models and also salt with the ocean model (CICE Consortium 2017; Madec et al. 2017).

2.2 Experimental design of the coupled PPE experiment

The detailed experimental design of the coupled PPE experiment (COUPLED) used to make the UKCP18 land projections is described in Yamazaki et al. (2021). Here we reiterate parts of the experimental design particularly relevant to this study. The experiment comprised five phases (Fig. 1), namely the calibration and spinup phases using a single model of the standard parameter configuration (STD) of GC3.05, followed by the spinup, historical and RCP8.5 scenario phases; some members dropped out due to instability or excluded due to excessively weakened AMOC so that the three phases had different ensemble sizes of 25, 24, and 22 respectively (Yamazaki et al. 2021). The original PPE consisted of one member which was the STD model itself and 24 perturbed parameter variants thereof. In all, 47 parameters

Fig. 1 Timeseries of the AMOC transport at 26°N from different phases of the UKCP18 COUPLED experiment. Black, gray and red lines denote STD, members included in the final projection and members excluded from the final projection, respectively



in the atmosphere and land components were perturbed, but we did not perturb any parameters in the ocean or sea-ice components. The parameter selection process is described in detail in Sexton et al. (2021). The PPE members are distinguished by 4-digit numbers. These numbers are inherited from the preceding 500-member atmosphere-only experiment (described in Sect. 2.5), in which each parameter perturbation combination was assigned a 4-digit number. The members in COUPLED inherit 25 of these numbers as well as the parameter perturbations. The number for STD is 0000, which is used to indicate STD in the figures.

2.3 Flux adjustment

A particular point of note is that in COUPLED, we employed flux adjustment. Because the surface climate plays a large role in determining regional climate projections, preventing the modelled sea surface temperature (SST) from drifting too far from the realistic climate was crucial. To this end, we applied three types of flux adjustment. One was the gridbox-wise damping heat flux derived in the calibration phase of the STD member, which was run under constant early-industrial external forcing with seasonal cycle. In the calibration phase, SST was restored to early-industrial climatology via the addition of artificial ocean surface heat flux calculated at each timestep. This damping heat flux was saved, time-averaged while preserving seasonal cycle and applied in conjunction with modelled surface heat flux in subsequent phases to all model variants. The next was the globally uniform damping heat flux, the value of which was unique to each ensemble member. The uniform damping heat flux was derived for each member from the global mean net top-of-the-atmosphere (TOA) radiative flux during their respective atmosphere-land-only PPE simulations used in the parameter selection stage (Sexton et al. 2021) prior to the coupled PPE experiment. Finally, gridbox-wise damping salt flux, also calculated in the calibration phase of STD while restoring sea surface salinity (SSS) to its early-industrial climatology, was converted to freshwater flux and processed in a manner similar to the gridbox-wise damping heat flux described above and applied as gridbox-wise damping freshwater flux with seasonal cycle in the subsequent experimental phases to all PPE members.

2.4 Experimental design of the current study

As stated in the Introduction, of the five-phase COUPLED experiment (Fig. 1), we focus on the spinup phase, at the onset of which the 25-member PPE was “unleashed”. The initial transient responses to the respective parameter perturbations, as captured in Fig. 1 as the fanning out of the AMOC transport, eventually led to each PPE member’s respective mean climate state. The goal of this study is to

predict the later-stage strength of the AMOC, measured by its transport, using earlier information from other ocean properties. Because the AMOC is an autocorrelated process, using information from other ocean properties from earlier times before the change in the AMOC has had the time to affect itself, is crucial. To this end, in this study, we first correlate the AMOC transport averaged over the final 20 years and other key ocean properties averaged over the initial 10 years to pick out features from the early-stage ocean properties that are associated with the later-stage AMOC strength. Secondly, we build multivariate regression model of the AMOC transport, using the identified features as predictors and compare modelled (or “predicted”) and actual AMOC transports. Finally, we apply this method to two datasets from other experiments to explore wider application. Specific details are described in Sect. 3. Furthermore, we conduct detailed analysis of the PPE data to ascertain physical mechanisms that underpin the relationship between the predictors and the AMOC strength in Sect. 4.

2.5 Description of the range of AMOC behaviour seen in the coupled PPE experiment and definition of members with stronger and weaker AMOC

Before we determine our predictors for predicting the AMOC strength after the model has spun up, it first helps to classify the behaviour in the AMOC at 26°N we see at the end of our historical simulations, where we have direct observations (Moat et al. 2022). In our analysis, the AMOC strength at 26°N is calculated as the vertical maximum of volume transport at this latitude. The volume transport in turn is calculated as the vertical cumulative sum of zonally integrated meridional velocity across the Atlantic basin. We categorise the 25 PPE members in the UKCP18 coupled experiment (Yamazaki et al. 2021) into two groups (Fig. 1, Fig S1). The criterion is their inclusion in the UKCP projections, which was in turn based on their AMOC and associated behaviour during the historical experiment as described in Sect. 1. The PPE members that were included in the UKCP projections are placed in the “members with stronger AMOC” group, except for members 2305 and 2335, whose AMOC weakened excessively during a separate, 200-year UKCP18 control experiment started from the spun-up state (Sexton et al. 2020). In contrast, the PPE members excluded from the UKCP projections are classified as “members with weaker AMOC”, except for members 0696 and 0103. The reason for their exclusion from the UKCP projection was persistent instability during the historical phase, but their AMOC transport was at par with members in the stronger/weaker AMOC group, so we place them in the respective groups (Table 1).

Table 1 PPE members in stronger and weaker AMOC groups

	Used in UKCP18 projection	Used in UKCP18 projection but weakened in early-industrial control experiment	Excluded from UKCP18 projection
Stronger AMOC	2123, 0834, 1843, 2242, 1935, 2491, 1649, 2832, 0605, 1554, 2868, 0000, 1113		0696
Weaker AMOC		2305, 2335	0090, 2753, 2089, 2914, 2884, 0939, 2549, 2829, 0103

In the final projection product of UKCP18, 13 of the 14 members with stronger AMOC (one member, 0696, was dropped as its historical simulation took too long to complete due to persistent instabilities) and two of the 10 members with weaker AMOC, 2305 and 2335, were included. The latter two members were included because their AMOC transport was relatively low but appeared to be levelling off at the end of the historical period

The above categorisation roughly corresponds with the strength of the AMOC at the end of the spinup phase, which precedes the historical experiment. That is, members that did not exhibit substantial reduction in the AMOC strength at the end of the historical experiment tended to have stronger AMOC at the end of the preceding spinup phase, and vice versa. The steady reduction of the AMOC in the historical phase in the majority of members with weaker AMOC was aided by the suppression of convection due to sea-ice cover encroaching over the deep convection region in the Subpolar Gyre (SPG) as the historical phase progressed (Fig S3 a,b show composite maps of sea-ice extent during the historical phase in members with weaker and stronger AMOC, respectively. Lin et al. (2023) show this occurring in CMIP6 models). These members, however, entered this regime, in which sea-ice cover had positive feedback on the AMOC reduction, because of the AMOC weakening initiated by other physical mechanisms during the spinup phase. For this reason, we hereafter focus on the spinup phase (hereafter referred to as COUPLED-spinup) and use the AMOC strength at 26°N averaged over the final 20 years for each PPE member as the representative value of the strength of the AMOC for that member, and one which we aim to predict. (The AMOC strengths at other latitudes averaged over the final 20 years of each member correlates highly with that at 26°N.) There are 15 and 10 members in the group with stronger and weaker AMOC, respectively (Table 1).

2.6 Other data from the UKCP18 project analysed in this study

In this study, to test whether this method can be applied more widely at an even earlier stage in the project, we also analysed two other archived datasets. One was produced in an experiment using only the atmosphere and land components, both at reduced resolution, conducted during the parameter selection process of the UKCP18 project. This experiment (hereafter referred to as “ATMOS”) was run for two years under historical forcing except for aerosol

emissions, which was prescribed at the pre-industrial level (Sexton et al. 2021). Data from this experiment was used in the current study to show the effect of the parameter perturbations without the influence of the coupling and to test how well the strength of the AMOC at the end of COUPLED-spinup could be predicted based only on data from the ATMOS framework.

The other dataset was produced in a PPE experiment with an identical setup to COUPLED, but without using flux adjustment. This experiment (hereafter referred to as “noFA-COUPLED”) was run for approximately 50 years under constant early-industrial forcing with seasonal cycle. Annual mean data is used in the analyses unless otherwise stated.

3 Methodology to predict the AMOC strength in the coupled PPE

3.1 Relationship of the AMOC strength and ocean properties

Many studies have found correlation between the AMOC transport and potential density in the SPG (e.g. Thorpe et al. 2001; Menary et al. 2013; Robson et al. 2014 and references therein). We exploit this relationship and look for the mechanism of the change in potential density, in a wider domain to take into consideration ocean advection from remote regions into the SPG region, in order to identify the cause of the change in the AMOC transport, in particular its reduction. Furthermore, since we did not perturb ocean parameters, the spread in the AMOC strength among the PPE members would have stemmed from the perturbations to the parameters in the atmosphere-land components, which in turn would have modulated the ocean temperature, salinity and velocity via the exchange of heat, freshwater and momentum fluxes at the atmosphere-ocean interface, as indicated in the ocean tracer and momentum equations. Here we investigate the surface fluxes of heat, freshwater and momentum as potential drivers. Depending on the experimental design of

the PPE, other potential drivers may be appropriate. Examining the change in potential density has the benefit that part of the change can be readily traced to changes in the surface fluxes, by examining changes in ocean temperature and salinity.

As the first step in this approach, we found that stronger AMOC (i.e. greater AMOC transport) at the end of COUPLED-spinup correlates well with higher potential density in the initial 10 years of COUPLED-spinup in the following locations. Namely, the upper 1000 m and deep (below 1000 m) ocean in the SPG, the upper 1000 m in the Arctic Ocean and the upper 1000 m in the Tropical North Atlantic Ocean (Fig. 2a,b). The domain identification was supported by the knowledge of the location and the direction of strong ocean currents (described in Sect. 4.2). Furthermore, in the SPG, the higher potential density in the initial 10 years is found to be driven by the cooler ocean temperatures, not higher salinities (compare Fig. 2c with 2e).

Next, we correlated the final AMOC with the heat and freshwater fluxes in the first 10 years of the spinup phase. In the version of the NEMO ocean model in the GCM used in this study, the surface heat flux consists of surface heat fluxes received from the atmosphere model, heat flux from sea-ice processes, heat flux arising from river outflow to the ocean, ice shelf processes and flux adjustment. On the other hand, the surface freshwater flux consists of evaporation minus precipitation, river outflow, freshwater fluxes from freezing and melting of sea ice, ice shelf processes and flux adjustment. Stronger AMOC at the end of COUPLED-spinup was also found to correlate well with initial 10-year average surface heat loss and freshwater loss fluxes in particular regions. We will later show in Sect. 4 that these regional fluxes affect the temperature and salinity and these signals propagate to the SPG where they affect the AMOC. These potentially physically meaningful regional fluxes with strong correlation ($p < 0.1\%$) with the AMOC strength are heat loss (i.e. heat flux out of sea) in SPG (Fig. 3a) and freshwater loss (i.e. freshwater flux out of sea) in the Arctic and the tropical North Atlantic Oceans (Fig. 3b). Finally, we exploit these correlations and define four regions (Fig. 3c). One is in SPG (Fig. 3c, coloured in green) where the AMOC strength is both positively correlated with surface heat loss (Fig. 3a) and negatively correlated with SST (Fig S4). The other three regions are where the AMOC strength is positively correlated with surface freshwater loss (Fig. 3b) in the Arctic, Tropical North Atlantic and the Amazon and Orinoco River outflow points (Fig. 3c coloured in red, blue and magenta, respectively). The Tropical North Atlantic region, though it appears relatively small in Fig. 3c, comprises 202 gridboxes (a close-up of the region is shown in Fig. 3e in blue). The region also coincides with the area where evaporation exceeds precipitation in COUPLED-spinup (Fig. 3d) and area of high negative correlation between summer

evaporation minus precipitation and the AMOC strength in ATMOS (Fig S5d) and area of high positive correlation between annual freshwater loss and the AMOC strength in noFA-COUPLED (Fig S5f). The Amazon-Orinoco River outflow region comprises just 41 gridpoints (a close-up of the region is shown in Fig. 3e in magenta), but the smallness of the number does not matter as these ocean gridpoints are part of the river outflow and these points realistically represent the magnitude of the river outflow from these two major rivers.

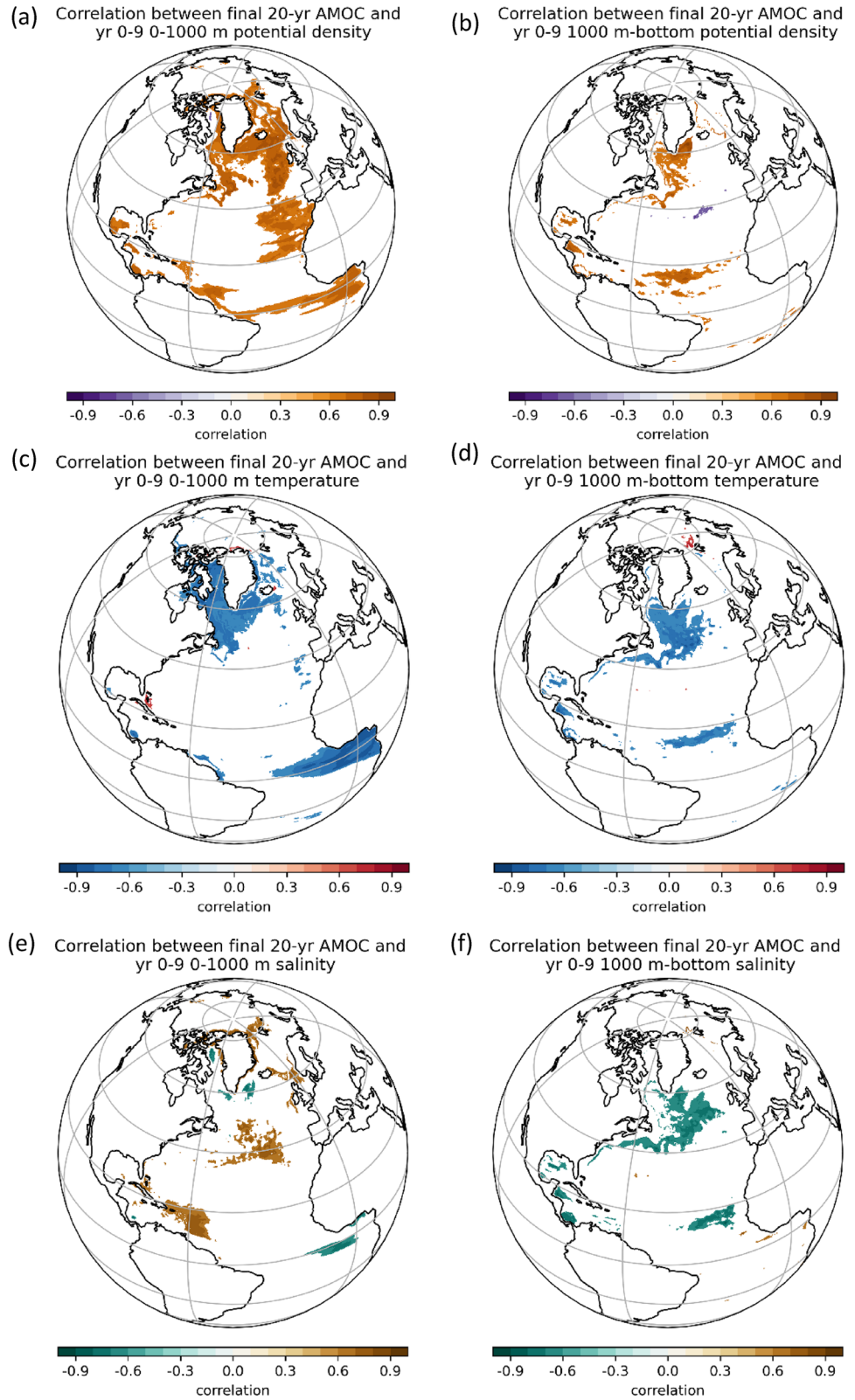
We have also correlated the final AMOC with the initial zonal and meridional wind stress. We found that the correlations were significant at the 0.1% level in four regions at around 20 N and one region at 40 N in the North Atlantic Ocean and over the Labrador Sea (not shown). None of these, however, were statistically significant as predictors in the multivariate regression model at the 5% level when assessed in conjunction with the four other predictors (i.e. SPG heat flux and the three freshwater regional fluxes) as a result of applying the stepwise regression method. The details of the multivariate regression analysis including stepwise regression are described in the next section.

The smallness of the ensemble size may be of concern, as it might result in spurious correlations. To check for this, we have examined the identified drivers and associated physical processes in detail in Sect. 4 and found that all of the identified drivers to be physically credible.

3.2 Predictions exploiting the relationships

The next step in the proposed method is to derive a predictive model of the AMOC based on the drivers identified in the previous section. To build the predictive model, we employed multivariate regression analysis. We calculated region-average values of the identified drivers over the critical regions as potential predictors and used a forward approach in stepwise regression method to check for statistical significance of each potential predictor. The procedure of the forward approach in stepwise regression is as follows. First, a regression model with a single predictor is formed for each potential predictor, for which the p-value is calculated. As a result, we obtain a p-value for each potential predictor. Next, multivariate regression model is gradually built up, by adding potential predictors one by one in the ascending order of the corresponding p-values. After each addition, p-values for the predictors in the multivariate regression model at that point are calculated. If the p-value of any of the predictors are larger than a pre-determined level, for which 5% was used in this study, that predictor is excluded from the multivariate regression model. The final multivariate regression model consisted of four predictors, namely the net freshwater loss in the Arctic, net surface heat loss in SPG, net freshwater loss in the Tropical North Atlantic,

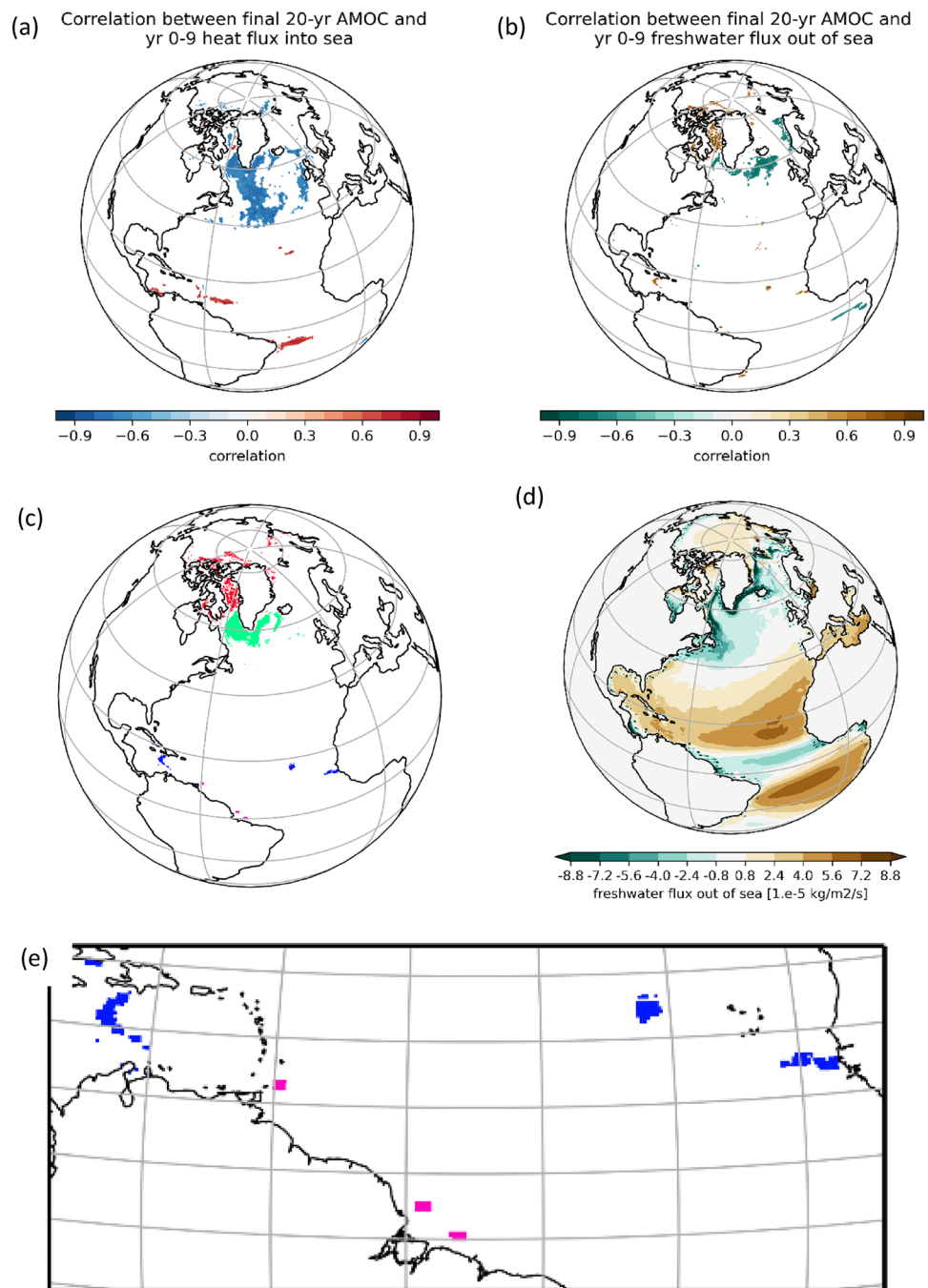
Fig. 2 Spearman's rank correlation coefficient in the 25 PPE members between ocean (a, b) potential density, (c, d) potential temperature, (e, f) salinity averaged over the first 10 years of COUPLED- spinup and the AMOC transport at 26 N averaged over the final 20 years of COUPLED-spinup. The variables in used in the calculation of correlation in (a, c, e) and (b, d, e) are integrated over the top 1000 m and from 1000 m depth to the bottom, respectively. The coefficient where correlation was significant at the 0.1% level is shown



and river outflow from the Amazon and Orinoco Rivers. The resulting predictive model for this PPE is expressed as follows:

$$Y_{AMOC} = \beta_0 + \beta_{Arctic_water} X_{Arctic_water} + \beta_{SPG_heat} X_{SPG_heat} + \beta_{Tropical_NAtlantic_water} X_{Tropical_NAtlantic_water} + \beta_{Amazon_Orinoco_runoff} X_{Amazon_Orinoco_runoff} \quad (1)$$

Fig. 3 Spearman's rank correlation coefficient between initial 10-year average **a** heat flux into sea and **b** freshwater flux out of sea and the final-20 year average AMOC transport at 26°N of COUPLED-spinup. The coefficient where correlation was significant at the 0.1% level is shown. **c** Four regions over which the initial 10-year average heat and freshwater fluxes of COUPLED-spinup are area-averaged and used as predictors in the multivariate regression model. Red, green, blue and magenta-coloured domains denote Arctic, SPG, Tropical North Atlantic and Amazon and Orinoco River outflow regions, respectively. **d** Freshwater flux out of sea in STD, averaged over years 0–9. **e** A zoomed-in version of **c** showing the Tropical North Atlantic region (blue) and Amazon and Orinoco region (magenta)



where Y_{AMOC} is predictand, X are predictors, β are the coefficients thereof and β_0 is the intercept.

Figure 4 shows the performance of various predictions but they all use essentially the same statistical model.

We formed two models based on Eq. 1 by specifying as predictands the AMOC strength averaged over a) the final 20 years (hereafter referred to as “base model”) and b) years 10–29. These models predicted (i.e. modelled) the AMOC strength in both the final 20 years and in years 10–29 very well (Fig. 4 a,b). (The correlation of predicted and actual

AMOC strengths was 0.97 and 0.95 and the adjusted R^2 was 0.919 and 0.879, respectively. The p-value for the F-test, i.e. the overall significance of the regression model, was $p < 0.01$ for both models.)

The coefficient, t-statistic and p-value of each predictor in predicting the AMOC strength averaged over each period are shown in Table 2. For the AMOC strength in the early years the SPG heat loss was the dominant predictor and the Amazon-Orinoco runoff was not statistically significant as a predictor (the latter was excluded from the model in the

stepwise regression stage), but for the AMOC in the final 20 year the Amazon-Orinoco runoff and the Arctic freshwater loss were the dominant predictors. This transition in the dominant predictors suggests that there are lags in the signals of the different regional fluxes to reach the SPG.

To test whether this prediction method could be more widely applied to a non-flux-adjusted PPE, the multivariate regression analysis was also carried out using data from the noFA-COUPLED experiment under constant early-industrial forcing, using the AMOC transport averaged over the final 20 years as the predictand. For predictors, the net heat loss in SPG and net freshwater loss in the Arctic region, averaged over the first 10 years in the corresponding regions as used in the COUPLED-spinup experiment, were selected as significant factors using the stepwise forward selection approach of stepwise regression. Thus the regression coefficients and the intercept were newly calculated. The multivariate regression model was statistically significant (p-value for the F-test was $p < 0.01$). The prediction worked here as well (correlation of predicted and actual was 0.96 and the adjusted R^2 was 0.84) (Fig. 4c).

To explore if the prediction method could be used at an earlier, parameter selection stage of the project prior to actually running the coupled PPE, the multivariate regression analysis was similarly performed using data from the ATMOS experiment as predictors. The AMOC transport at the end of COUPLED-spinup was used as predictand and the predictors were the Arctic air temperature, northern South American surface and subsurface runoff and Tropical North Atlantic evaporation minus precipitation from the ATMOS experiment averaged over the entire simulation (2 years). The first variable was chosen as proxy to both the SPG heat loss and Arctic freshwater loss used to predict AMOC in COUPLED-spinup, as these variables are not physically meaningful in the ATMOS experiment, in which SST and sea-ice area were prescribed. The regions the predictands were averaged over were determined by performing correlations between the AMOC averaged over the final 20 years of the COUPLED-spinup experiment and the variables from the ATMOS experiment. The area-averaged variables were validated using the stepwise forward selection approach of stepwise regression. The multivariate regression model using the above three predictors was significant (p-value for the F-test was $p < 0.01$) and predicted the AMOC strength in the final 20 years of COUPLED-spinup well (correlation of predicted and actual was 0.86 and the adjusted R^2 was 0.696) (Fig. 4d). The coefficient, t-statistic and p-value of each predictor in predicting the AMOC strength averaged over each period are shown in Table 2.

To evaluate the performance of the multivariate regression model when given data for a new PPE member, we conducted a leave-one-out cross validation. This was executed by forming the multivariate regression model with one member excluded, then using the resultant model to predict the

AMOC strength of the excluded member. The procedure was repeated one by one for all members. Figure 4e shows the predictions made via the leave-one-out cross validation, which are very similar to those shown in Fig. 4a. The adjusted R^2 for the predictions via the leave-one-out cross validation was 0.883, so we conclude that the high adjusted R^2 value of 0.919 of the original model is not due to overfitting and that it is suitable for making predictions with new data.

Although not demonstrated in this paper using examples, in practice, the multivariate regression model trained as described above can be employed to predict the AMOC strength at a later period of additional perturbed parameter members (with different parameter perturbations to the original 25 members), after running them for 10 years under the COUPLED-spinup framework. To utilise the predictions to determine and select members to retain and drop, we would choose a threshold below which we would stop the simulation early. As we are currently concerned with effects of AMOC that is too weak, we could select members with AMOC stronger than 13 Sv. For the sake of illustration, supposing for now that the prediction in Fig. 4a have been made for the hypothetical additional members, members 2884 and 2305 would be false negatives and member 0939 would be a false positive. For prediction of AMOC based on a non-flux adjusted coupled PPE (using Fig. 4c) or on atmosphere-only experiments (Fig. 4d), the relationships are slightly weaker so we would expect the rate of false rejections to increase slightly.

In summary, the method of predicting later-period AMOC strength by multivariate regression using early-period regional surface fluxes worked well, not only for COUPLED but also for noFA-COUPLED and ATMOS experiments, showing promise for wider application.

In the following section, we describe the physical mechanisms of how these fluxes affect the AMOC strength.

4 The mechanisms of the AMOC changes in the coupled PPE

In this section, we investigate the physical mechanisms that underpin the choice of predictors in Sect. 3, i.e. heat and freshwater fluxes in the four critical regions (Fig. 3c). The schematic diagram shown in Fig. 5 summarises the causal relationships between the mechanisms described in this section and the AMOC transport in the AMOC-weakening members.

4.1 Mechanisms at work in SPG

In the initial 10 years of COUPLED-spinup, members with stronger AMOC are linked with both the cooler ocean temperature (Fig. 2c, Fig S4) and the larger surface heat loss in SPG (Fig. 3a). This means that most of the larger surface

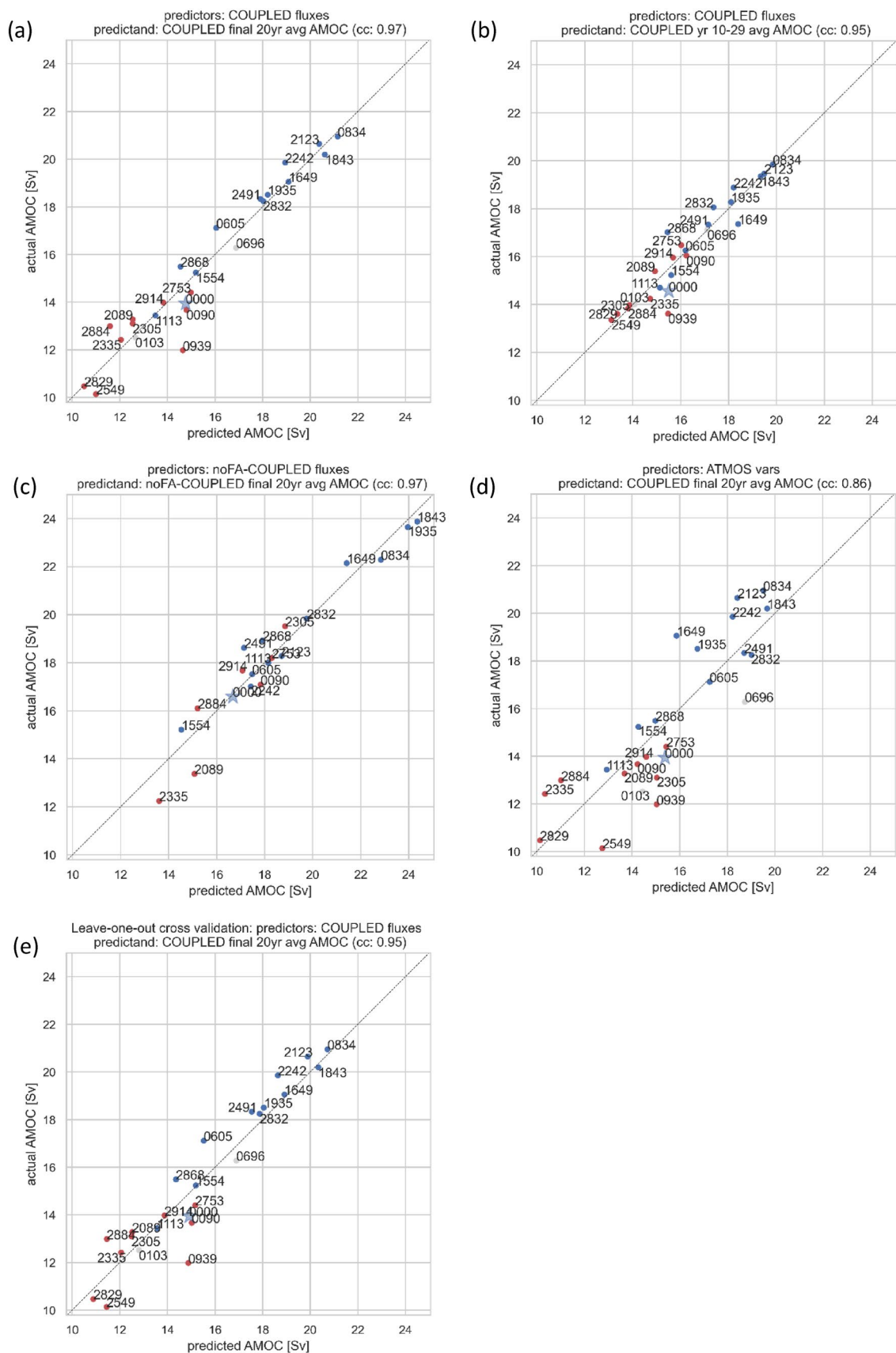


Fig. 4 Predicted and actual AMOC transport at 26°N. Predictors and predictand in the multivariate regression model are: **a** fluxes in the first 10 years of COUPLED-spinup and AMOC in the final 20 years of COUPLED-spinup, **b** fluxes in the first 10 years of COUPLED-spinup and AMOC in years 10–29 of COUPLED-spinup, **c** fluxes in the first 10 years of noFA-COUPLED and AMOC in the final 20 years of noFA-COUPLED and **d** variables in years 0–1 of ATMOS and AMOC in the final 20 years of COUPLED-spinup experiments, **e** same as **a** but result of leave-one-out cross validation, respectively. The correlations are **a** 0.97, **b** 0.95, **c** 0.97, **d** 0.86 and **e** 0.95, respectively. **a**, **b**, **d**, **e** comprise 25 members whilst **c** comprises 20 members. Blue/red dots and star (STD) indicate members with stronger/weaker AMOC in the COUPLED experiment. Only the predictors that were statistically significant were included in the respective multivariate regression models, as follows: **a**, **e** SPG heat flux, Arctic and Tropical North Atlantic freshwater fluxes and Amazon-Orinoco River runoff, **b** SPG heat flux and Arctic and Tropical North Atlantic freshwater fluxes, **c** SPG heat flux and Arctic freshwater flux and **d** Arctic surface air temperature, Tropical Atlantic precipitation minus evaporation and northern South American surface and subsurface river runoff, respectively. The leave-one-out cross validation was performed by forming the multivariate regression model with one member excluded, then using the resulting model to predict the AMOC strength of the excluded member. The procedure was repeated for all members. Predictions thus made are plotted in **e**

heat loss is not a consequence of a warmer ocean temperature stemming from stronger AMOC transporting more heat into the region but rather the predominant cause of the cooler ocean. Hence, it makes sense to examine this larger surface heat loss further.

The course of events occurring in a typical member with stronger AMOC is described below. The description is based on the following evidence: timeseries of SPG ocean temperature, salinity and potential density in the upper 1000 m (Fig. 6 a–f) and the deep ocean (1000 m—bottom) (Fig. 6 g–l), timeseries of net heat flux into sea and mixed layer depth in SPG (Fig. 6 m,p), the amount of freshwater loss and heat loss in the four critical regions in the first 10 years (Fig. S2a–d), the yearly composite anomaly maps of SSS and upper ocean salinity (Figs. S7, S8), correlation of precipitation flux with the AMOC strength (Fig. S5e), a map showing freshwater gain from sea-ice growth at the sea-ice edge (Fig. S6b) and the spread in the individual components of the air-sea heat flux (Fig. 7). The response to the parameter perturbations of an AMOC-strengthening member develops in the following order:

- The increased surface heat loss in SPG (Fig. 6p) cools the upper ocean (Fig. 6a). It also becomes fresher (Fig. 6e) due primarily to increased precipitation in eastern SPG (Fig. S5e) and an increase in freshwater from ice melt at the sea-ice edge front in the Labrador Sea that accompanies sea-ice growth at the sea-ice edge (Fig. S6b).
- The upper ocean water in SPG becomes denser (Fig. 6c) primarily from the cooling
- Stronger deep convections occur (mixed layer depth in Fig. 6m) and the water in deep SPG becomes cooler, fresher and denser (Fig. 6j–l)
- The AMOC strengthens (Fig. S1, blue lines)
- Meanwhile, Arctic Ocean loses freshwater (Fig. S2c) mainly from increased freezing and becomes more saline. The more saline water is transported to SPG
- Furthermore, water in the tropical North Atlantic Ocean regions becomes more saline (Figs. S7 and Fig. S8) due to freshwater loss in these regions (Figs. S2 a,b). This more saline water is transported poleward
- More heat and salt are advected into SPG (Fig. 8 b,a), the latter being due to both the increased poleward mass transport and the increased salinity in the water in the Arctic and the tropical North Atlantic
- SPG water becomes warmer but more saline and consequently denser (Fig. 6a–c). The AMOC strengthens further (Fig. S1 blue lines except 1113 and 1554)
- The AMOC stabilises at a level where the opposing feedbacks from the warmer temperature, higher salinity and cooling by local heat loss all balance in setting the density, which drives the deep convection (Fig. 6a–c, g–i). Additionally, the warmer surface temperature results in more heat loss by sensible heat flux (Fig. 7)

In contrast, members with weaker AMOC can be divided into roughly three groups. The AMOC in the first group weakens steadily from the start of COUPLED-spinup (2549, 2884, 2829, 0939). In the second group the AMOC oscillates around the same level for the first 30–40 years then steadily weakens (2089, 2305, 2335). The AMOC in the third group strengthens during the first 30 years or so then flips to a steady decline (0090, 2753, 2914). The response of the first, steadily weakening group is the direct opposite to the response of the strengthening AMOC group described in steps above.

On the other hand, the density in SPG in members in the second and third groups remains steady (second group) or even increases (third group, Fig. S13c) in the first 30 years or so, depending on the competition primarily between SPG heat gain/loss and more saline/fresher water transported from the Arctic. Thereafter the AMOC declines in both groups, due to the arrival of fresher water transported into SPG from the tropical North Atlantic regions, wherein there are large increases in freshwater. Annual salinity anomaly maps (Fig. S10) for a member in the third group, 2753, expose the gradual competition between increased salinity originating in the Arctic Ocean and the reduced salinity originating in the Amazon and Orinoco River outflow and the Tropical North Atlantic regions.

Fig. S15 depicts how the different contributions change over time, by showing the magnitude (i.e. the absolute value)

Table 2 Statistics of respective predictors in the three and one multivariate regression models predicting the AMOC transport at 26 N in the COUPLED-spinup and noFA-COUPLED experiments, respectively

Predictors	Predictand					
Initial-10-year average COUPLED-spinup fluxes in the four regions	(a) COUPLED-spinup final 20-year average AMOC at 26 N (base model)			(b) COUPLED-spinup year 10–29 average AMOC at 26 N		
	Coefficient	t-statistic	p-value	Coefficient	t-statistic	p-value
Amazon-Orinoco River runoff	-0.9993	-3.833	0.001	-0.1698	-0.842	0.409
Tropical North Atlantic freshwater loss	0.6798	2.431	0.025	0.5369	2.483	0.022
Arctic freshwater loss	1.1458	3.678	0.001	0.6075	2.523	0.020
SPG heat loss	0.7349	2.297	0.033	0.8316	3.362	0.003
Initial-10-year average noFA-COUPLED fluxes in the two regions			(c) noFA-COUPLED final 20-year average AMOC at 26 N			
			Coefficient		t-statistic	p-value
Arctic freshwater loss			0.7250		2.388	0.029
SPG heat loss			2.2698		7.476	0.000
2-year average ATMOS fluxes in three regions	(d) COUPLED-spinup final 20-year year average AMOC at 26 N					
	coefficient		t-statistic		p-value	
Northern South American surface and subsurface river runoff	-1.5469		-3.639		0.002	
Tropical North Atlantic precipitation minus evaporation	-0.9279		-2.347		0.029	
Arctic surface air temperature	-0.9811		-2.198		0.039	

Notations a-d in the table correspond to those of the subfigures in Fig. 4. Numbers in bold indicate low p-value (<0.05) and thus that the predictor is a meaningful addition to the analysis. The critical regions the fluxes were averaged over for the multivariate regression model using noFA-COUPLED data (b) is the same as those for the “base model” (a). The critical regions the fluxes were averaged over for the multivariate regression model using ATMOS data (d) have been derived for the ATMOS data using correlation between ATMOS fluxes and the AMOC strength in the final 20 years of COUPLED-spinup

of the coefficients of the multivariate regression model described in Sect. 3, but here by varying the predictand with time. The predictors are the same first 10-year average heat and freshwater fluxes in the four regions described in Sect. 3. The predictand is the AMOC strength averaged over successive periods defined by a sliding 20-year window, starting from the 11th year. In Fig. S15, only coefficients of predictors that are significant ($p < 0.05$) are plotted for any one year. Initially, there are just three significant predictors, with the SPG heat flux dominating. After about 50 years, the contribution from the Arctic freshwater flux dominates, followed by that from the Amazon-Orinoco River runoff, which becomes significant only after about 45 years.

To scrutinise the triggering events within the SPG described earlier, we quantify the relative contributions of the heat budget components. We considered the temperature tendency equation for the upper 0–1000 m ocean in SPG:

$$\frac{\partial T}{\partial t} = \frac{1}{dc_p \rho_o} Q_{net} - \nabla(\mathbf{u} \cdot T) + R,$$

where T is potential temperature of the upper ocean, t is time, d is thickness, c_p is specific heat, ρ_o is seawater density, Q_{net} is the net surface heat flux into sea, \mathbf{u} is horizontal

velocity and R signifies the residual terms, which include contributions from vertical advection, horizontal and vertical diffusion and convection. The terms in the temperature tendency equation of the domain are calculated using data for each gridbox within SPG and taken volume-weighted average. We used archived monthly mean potential temperature and velocity for the calculation (Ivanova et al. 2012), because the monthly mean advection and diffusion term data were not archived. Therefore, the residual term also includes the sub-monthly products of the advection term. The time-series are shown in Fig. 7 for five typical members ((a,b) members with stronger AMOC, (c,d) members with weaker AMOC, (e) member with weaker AMOC that initially show a strengthening of the AMOC, (f) SPG 0–1000 m ocean volume-weighted average potential temperature for the five members; each timeseries in (f) is equivalent to the cumulative sum of the temperature tendency in each of (a-e).) The plots show the relative contributions of surface heat flux and heat advection (Fig. 7) and corroborates the course of events described earlier in this section. Namely, in the members with stronger AMOC, the advective component increases with time, while it decreases with time in the members with weaker AMOC (in 0090 the advective component increases

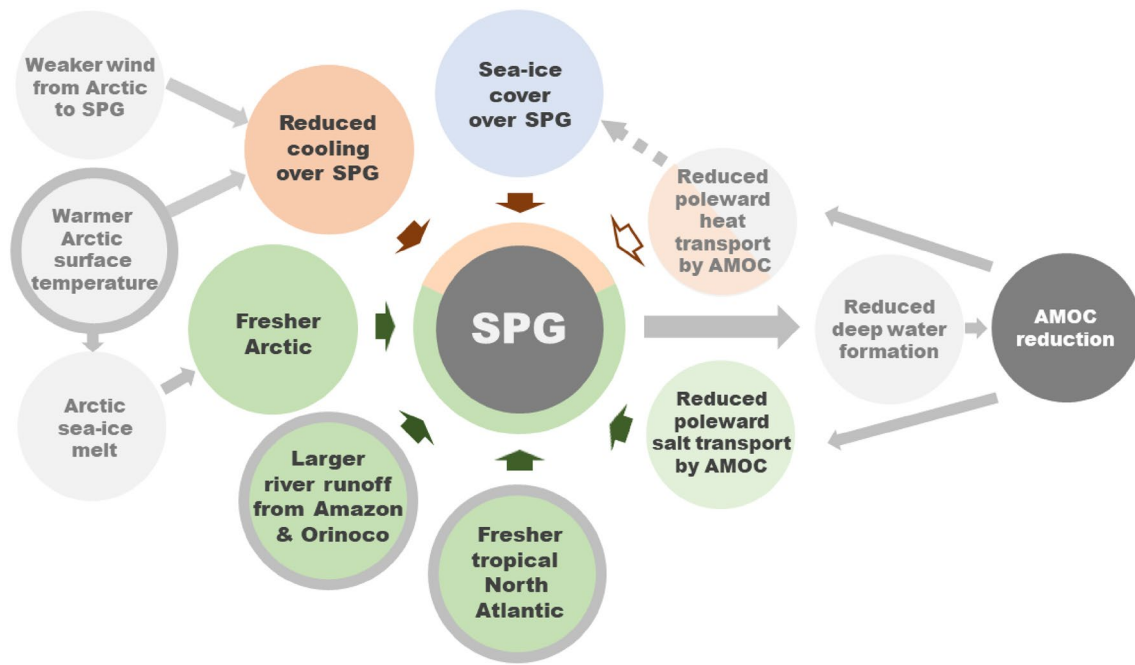


Fig. 5 Schematic diagram depicting how local and remote mechanisms work to reduce seawater density and hence/or deep-water formation in SPG and cause the AMOC to weaken in COUPLED experiment. Coloured filled circles indicate mechanisms that have direct influence on SPG density and/or deep-water formation; orange, green and blue circles indicate mechanisms associated with heat flux, freshwater flux and sea-ice cover, respectively. Darker orange and green circles represent the four mechanisms (here described with characteristics linked to AMOC reduction) used as predictors in the multi-

variate regression analysis to predict the AMOC strength. Pale gray circles denote mechanisms that affect SPG density indirectly. Circles with gray rings indicate triggering mechanisms that stem from parameter perturbations. Arrows indicate the direction of influence. Filled orange and green arrows indicate warming and freshening effects on SPG, respectively. Hollow orange arrow indicates cooling effect on SPG. The relative influence of the mechanisms varies across PPE members and shifts over time

for the first 40 years then decreases). As triggers for large positive values of the residual component (Fig. 7a–e) coincide with the timing of cooler temperatures (Fig. 7f), the dominant contribution to the residual component appears to be made by convection. The net surface heat flux does not vary very much over time, while the advective and the residual heat fluxes evolve over time. We conclude that the temperature tendency in the SPG is initially controlled by the local net surface heat flux (in approximately the initial 10 years), then modified by advection and other processes, corroborating the triggering events occurring in SPG described earlier.

What causes the increased surface heat loss in SPG in members with stronger AMOC? The anomalies of 0–9 year mean annual mean air-sea heat flux components from the corresponding components in the STD (Fig. 9) indicate that the difference between the spread in the stronger and weaker AMOC groups is largest in the sensible heat flux. What, then, increases heat loss by sensible heat flux in members with stronger AMOC? Sensible heat flux is proportional to windspeed and the difference in SST and air temperature. In SPG, stronger northerly (or weaker southerly) wind in winter and colder surface air temperature both correlate

with stronger AMOC (Fig. 10a,b). Composite difference (mean of members with stronger AMOC minus mean of members with weaker AMOC) map of air temperature advection (Fig. 11) indicates that there is anomalous advection of cold air from the Arctic over Greenland into SPG in members with stronger AMOC. This leads to greater temperature difference between the SST and air temperature and hence sensible heat flux in members with stronger AMOC. In the ATMOS results corresponding to the 25 PPE members, meridional surface wind and surface air temperature do indeed also correlate with the AMOC strength (Fig. 10c,d), although the former was not a statistically significant predictor in the multivariate regression model predicting AMOC in the COUPLED-spinup experiment.

4.2 Sources and roles of the freshwater flux in the tropical North Atlantic and the Arctic

In this subsection, we examine in more detail the sources and roles of the freshwater fluxes described in the previous subsection. In our model, in addition to the effect of the heat flux as discussed above, the density of seawater in SPG is strongly affected by the salinity in the inflow of seawater

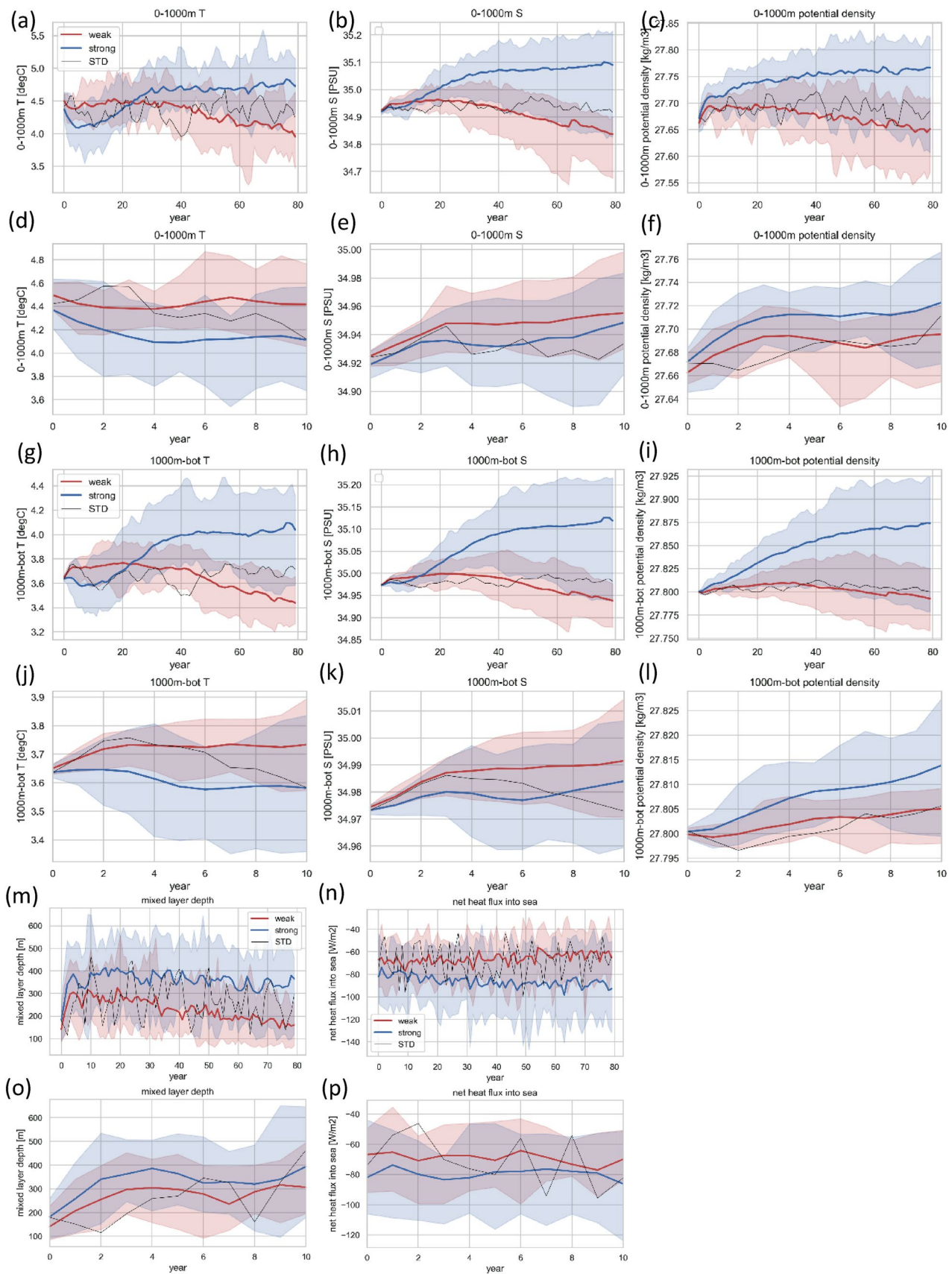


Fig. 6 Timeseries of annual mean potential temperature (a, d, g, j), salinity (b, e, h, k), potential density (c, f, i, l), mixed layer depth (m, o) and net surface heat flux into sea (n, p) in SPG in COUPLED-spinup. The mixed layer depth is area-weighted-average and the rest is volume-weighted-average over depth 0–1000 m (a–f) and 1000 m–bottom (g–l). Mean (line) and spread (shade) of PPE members with stronger and weaker AMOC transport at 26°N at the end of COUPLED-spinup are coloured in blue and red, respectively. STD member is coloured in black. a–c, g–i, m, n and d–f, j–l, o, p are plotted over the entire and the first 10 years of COUPLED-spinup, respectively

from two main sources. One is the westward-flowing SPG circulation of waters from the North Atlantic Current into the Irminger Sea. Through this route, tropical freshwater fluxes affect local salinity and this propagates to the SPG via the North Atlantic Current (Fig. S7). The other is the outflow from the Arctic Ocean through Davis and Hudson Straits into the Labrador Sea and through the Fram Strait over the Greenland-Iceland-Scotland (GIS) Ridge into the Irminger Sea. Arctic freshwater fluxes affect local salinity, which propagates to the SPG via the above pathways. The sources of the tropical and Arctic freshwater fluxes will be discussed next.

Firstly, in the tropical North Atlantic, there are two main sources of freshwater flux that ultimately affect salinity in SPG. One is the evaporation minus precipitation flux extending across the tropical North Atlantic and the other is the river outflow from the Amazon and Orinoco Rivers. The freshwater fluxes from the two sources appear to be related in members with very strong/weak AMOC in that there is more/less evaporation minus precipitation and less/more river outflow (Fig. S2 f and e). However, the relationship is not apparent in members with intermediate AMOC strengths. The geographical regions corresponding to these fluxes are shown in Fig. 3c in blue and magenta, respectively. The Tropical North Atlantic region lies within the domain where annual evaporation exceeds precipitation (Fig. 3d). Furthermore, in the eastern part of this region, i.e. off the African coast at approximately 20°N, the summer evaporation minus precipitation flux in ATMOS and annual freshwater loss in noFA-COUPLED both exhibit strong positive correlation with the AMOC strength as well (Fig S5d/S5f). This suggests that the amount of freshwater flux in this region can be traced to parameter perturbations, although it would also have been affected by the atmosphere–ocean coupled response. Regarding the second source, the Amazon and the Orinoco River outflow, it is proportional to the surface and subsurface river runoff, and thus precipitation minus evaporation, over land in the expansive river basin spanning northern South America (area encircled by the blue line in S5 a–d). The region where evaporation minus precipitation and the AMOC strength are lag-correlated within this river basin is qualitatively similar in the ATMOS and

COUPLED-spinup (Fig S5: compare (a) with (c) and (b) with (d)), which suggests that the amount of the outflow is dictated by parameter perturbations.

Secondly, with regard to the Arctic freshwater flux, the region where it is positively lag-correlated with the AMOC strength is shown in Fig. 3c in red. The Arctic freshwater flux consists of evaporation and precipitation over open sea, river runoff and decrease/increase in freshwater from freezing/melting of sea ice (freezing/melting results in decrease/increase in freshwater because freshwater is captured in/released from sea ice). Sea-ice processes are the largest component of the freshwater flux in the Arctic region in most of the members with stronger AMOC (Fig S14 a,c). Members with stronger AMOC also tend to have larger loss or smaller increase in surface freshwater and smaller river outflow in these regions (Fig S14d). Contribution from evaporation minus precipitation over open ocean (Fig S6a) is small overall (Fig S14a, magenta dots). When the more saline seawater is transported from the Arctic into SPG, density of water therein increases and promotes stronger deep convection, assisting the mechanism described in the previous subsection. The members with anomalously large freshwater loss in this region correspond to those with anomalously cool Arctic surface air temperature in this region (Fig. 10b), and also with anomalously larger amount of sea ice (Fig S14b). Member 2868, included in the stronger AMOC group, is an outlier in terms of the Arctic freshwater flux, which for this member was an increase in freshwater (Fig S2c). Instead, this member exhibited anomalous freshwater loss in SPG (Fig S11), which led to salinity increase and hence density increase in upper SPG water.

In summary, in COUPLED-spinup, freshwater fluxes in the critical regions in the Tropical North Atlantic Ocean, Amazon and Orinoco River outflows and the Arctic Ocean all modified local salinity, which was eventually transported to the SPG and transformed the density therein and affected the deep convection and hence the strength of the AMOC.

4.3 Roles of parameter perturbations

The 25 COUPLED PPE members were all chosen from a subset of roughly 500 ATMOS PPE members. As 500 is much greater than 47, the number of parameters that are perturbed, we can build emulators (statistical models trained on the PPE that can be used to predict model output at untried parameter combinations) and use them in a sensitivity analysis (e.g. Lee et al. 2013) to identify the most important parameters, which in turn indicate the key processes that drive variation in the AMOC across the coupled PPE. We use a Gaussian Process for the emulator and use the method of Saltelli et al. (1999) to estimate the fraction of the variance of the emulator's best-fit explained by each parameter

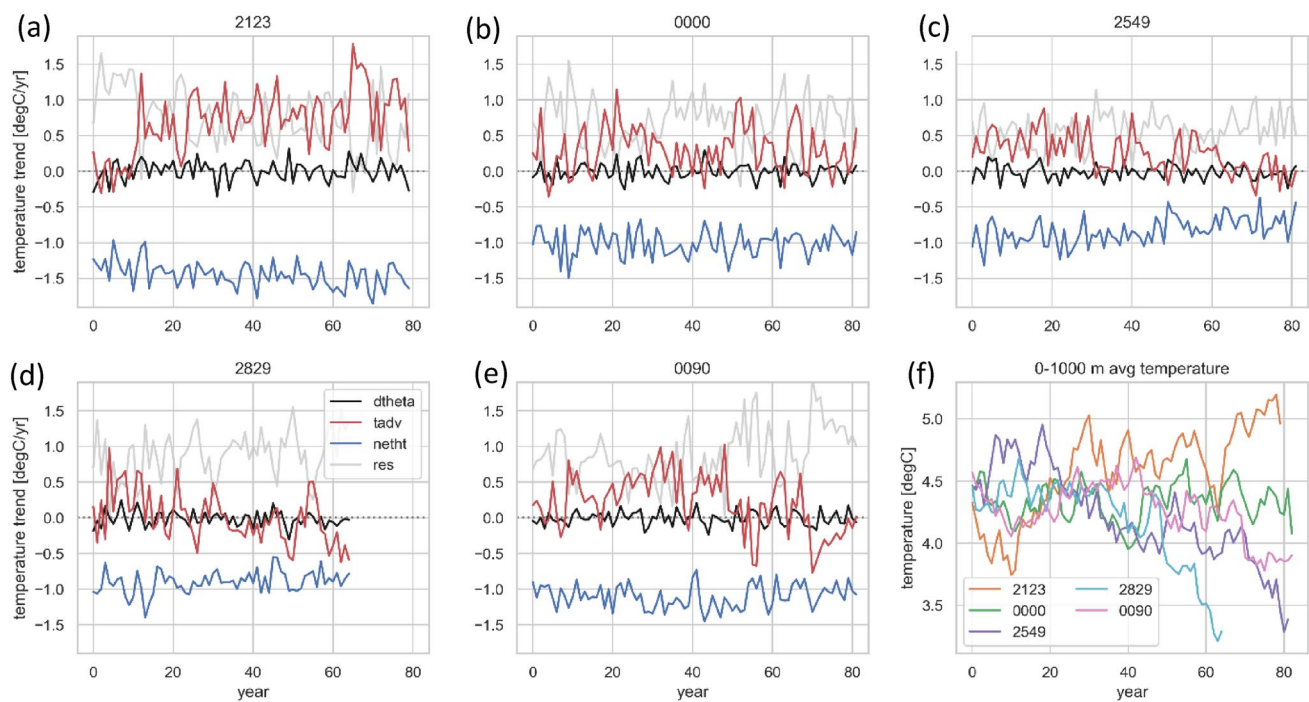


Fig. 7 Timeseries of the ocean potential temperature tendency equation terms, volume-weighted and averaged over depth 0–1000 m in SPG, for five typical PPE members in COUPLED-spinup. **a**, **b** members with stronger AMOC (2123 and STD), **c**, **d** members with weaker AMOC (2549 and 2829) and **e** member with weaker AMOC that initially show a strengthening of the AMOC (0090). Black, blue,

red and gray lines denote the temperature tendency, surface heat flux into ocean, advection and residual terms, respectively. **f** SPG area-weighted average, 0–1000 m average potential temperature for the five members shown in **a–e**. Each timeseries in **f** is equivalent to the cumulative sum of the temperature tendency in each of **a–e**

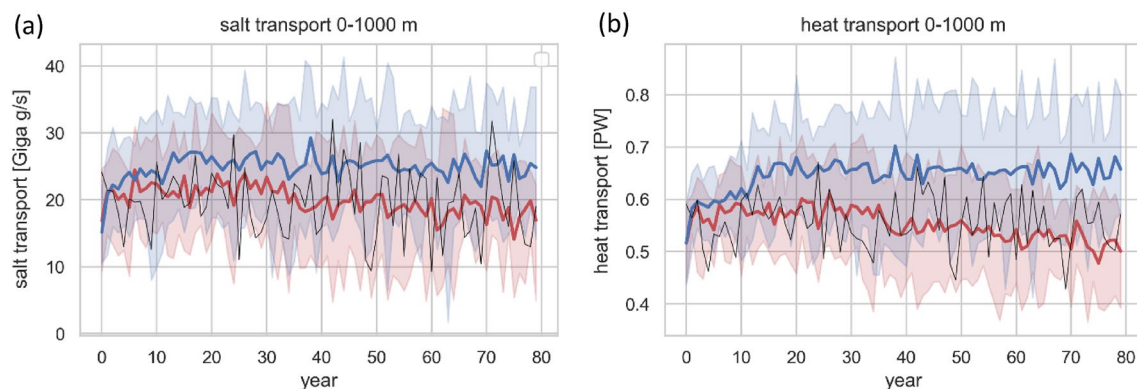


Fig. 8 Timeseries of zonally- and depth-integrated salt transport **a** and heat transport **b** across the Atlantic Ocean at 55N in COUPLED-spinup. Depth-weighted integration was performed over the upper 1000 m. Blue and red lines denote average of strong and weak

AMOC members, respectively. Pale blue and red shades indicate spread in strong and weak AMOC members, respectively. Black line denotes STD

for any model output; see Rostron et al. (2020) for more details.

We can only apply this to the variables in the ATMOS experiments that have been identified as relevant. For the Amazon-Orinoco runoff, a single parameter, the mid-level entrainment rate which controls the shape of the mass flux

and the sensitivity of mid-level convection to relative humidity, dominated by explaining nearly 70% of the variance across the ATMOS PPE. For Arctic temperature, various parameters in the cloud microphysics and gravity wave drag schemes contributed to the PPE spread, most notably, ai , which controls the density of cloud ice, explained about

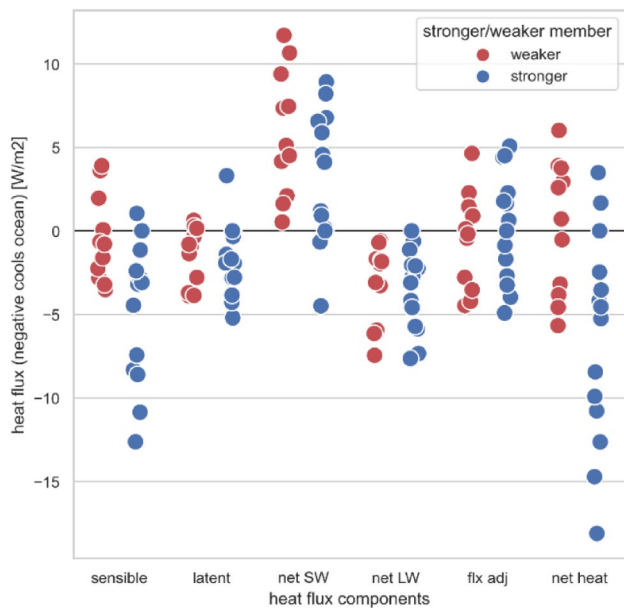


Fig. 9 The anomalies of surface heat flux components, averaged over the first 10 years of COUPLED-spinup, from the corresponding components in the STD. Blue and red dots denote members with stronger and weaker AMOC transport at 26°N at the end of COUPLED-spinup

40% of the variance. For precipitation minus evaporation over the Tropical North Atlantic region identified in Fig. 2c, there were modest contributions from entrainment and detrainment parameters in the convection scheme, the biomass burning emission flux, and from some gravity wave drag parameters. Overall, this shows that important drivers of the AMOC are sensitive to many parameters, making the AMOC a hard to variable to understand in the climate model.

5 Summary and discussion

We developed a method to diagnose the drivers of the AMOC strength in a PPE of a coupled GCM, and to predict the AMOC strength with a simple statistical model using the identified drivers as predictors. As an example, we applied this method to data from the spinup phase of a 25-member PPE HadGEM3-GC3.05 GCM experiment (COUPLED-spinup), in which the initial transient response of the modelled climate system to the parameter perturbations were captured. The drivers that control the strength of the AMOC in the later stage of the experiment were identified and the strength was predicted (modelled), based on the climate state of the initial decade, to a high accuracy. Specifically, to identify the drivers of the AMOC strength, we used a correlation analysis on the surface heat, freshwater and momentum fluxes, which were pre-selected by drawing on the PPE's experimental design. To predict the AMOC

transport, we formed a multivariate regression model, in which the drivers obtained in the previous step were used as predictors. Of these, heat flux in the SPG and freshwater flux in the Arctic and Tropical North Atlantic Oceans and from the runoff of Amazon and Orinoco Rivers were found to be statistically significant. These predictors were then shown to have physical underpinning in that the PPE members that exhibited AMOC weakening were revealed to possess some combination of the following characteristics: (i) anomalously warmer SPG, (ii) anomalously fresher Arctic Ocean, (iii) anomalously fresher Tropical North Atlantic Ocean, and (iv) anomalously larger runoff from the Amazon and Orinoco Rivers. These characteristics were broken down into further causes: (i) is the result of (a) anomalously warm surface Arctic temperature and/or (b) anomalously weak surface northerly wind in SPG, particularly in the Labrador Sea; (ii) is also the result of (a) through sea-ice melt; (iii) is the result of anomalous increase in freshwater from surface freshwater fluxes, which in turn is the result of (c) anomalous increase in freshwater from evaporation minus precipitation. Furthermore, it is likely that (a), (c) and (iv) stem, at least partially, from parameter perturbations because these features are present in the atmosphere-only model (ATMOS) results as well, whereas (b) is likely to be the result of atmosphere–ocean coupled response because we see no traceability of this aspect between ATMOS and COUPLED-spinup. The resultant change in the AMOC further feeds back onto the AMOC itself e.g. via reduced heat and salt transport, as the AMOC is an autocorrelated process. The mechanistic processes described here are summarised in a schematic diagram in Fig. 5. We also showed that ocean potential density in the upper SPG was a determining factor for the AMOC strength, as shown in many past modelling studies (e.g. Thorpe et al. 2001; Menary et al. 2013; Robson et al. 2014 and references therein). It is possible that the reason we did not observe the oscillation in the AMOC strength found in Vellinga and Wu (2004), in which salt accumulation in the tropics during the weak AMOC period eventually leads to the recovery of the AMOC strength, was because the freshening in the tropical North Atlantic inherent in members with weaker AMOC precluded salt accumulation in the tropics.

The method employed in this study, as far as we are aware, is novel, in that it allows the separation of the “effects of the drivers of AMOC change” from the “effects of the changed AMOC onto the drivers” and hence onto the AMOC itself. For example, if the SPG was found to be more saline in some models with stronger AMOC, it is usually not possible to tell if this was the cause of the stronger AMOC or the result of one. However, by using the PPE and comparing the drivers from the period immediately after the application of parameter perturbations (when the consequences of the AMOC transport change triggered by the perturbations had not yet

Fig. 10 Spearman's rank correlation coefficient in the 25 (a, b) COUPLED and (c, d) ATMOS PPE members between (a, c) meridional wind at 850 hPa and (b, d) surface air temperature, averaged over December, January, February and March of (a, b) the first 10 years of COUPLED-spinup and (c, d) the 2-year ATMOS experiment, and the AMOC transport at 26°N averaged over the final 20 years of COUPLED-spinup. Coefficient where correlation was significant at the 5% level is shown. This level is different to the significant level of 0.1% used in correlation plots in other Figures. This level was chosen to clearly show the relatively weaker signal of the correlation between the ATMOS fluxes and AMOC compared to that between COUPLED fluxes and AMOC

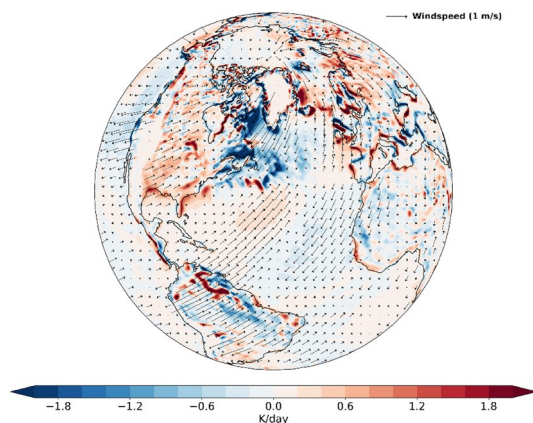
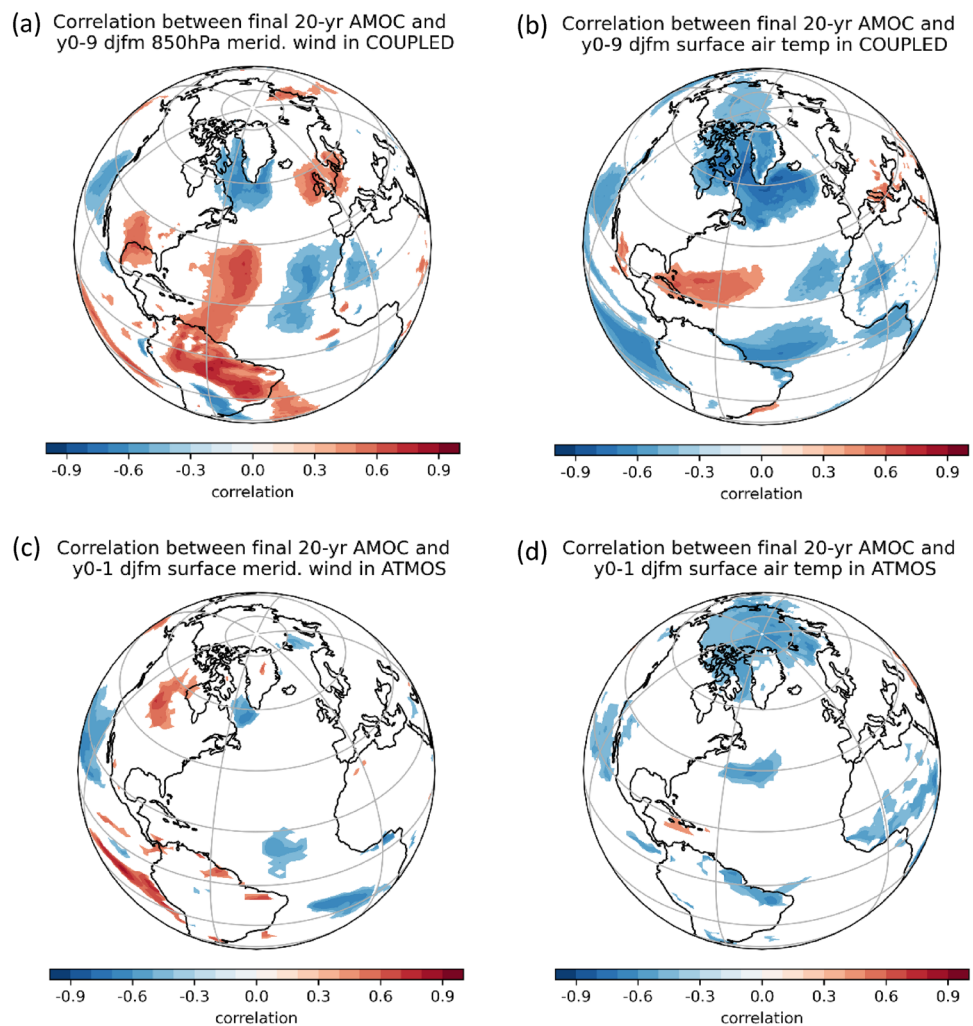


Fig. 11 Composite difference map (mean of members with stronger AMOC at the end of COUPLED-spinup minus mean of members with weaker AMOC at the end of COUPLED-spinup) of air temperature advection, averaged over the December, January and February of the first 10 years of COUPLED-spinup. Air temperature advection was calculated from archived monthly mean data of air temperature and horizontal wind at 850 hPa

reached SPG to feed back onto the drivers), with the AMOC transport several decades later, we were able to identify the drivers that caused the AMOC transport to change.

The predictors are derived from strong emergent relationships where there is a high correlation between a time-averaged variable from the start of the spinup with a time-averaged variable of interest from the end of the spinup. The emergent relationship comes from a PPE, where members differ due to parameter effects and internal variability but each share a common systematic error. This differs to a multimodel ensemble where there is a third source of variation, different systematic errors for different climate models which cannot be observed but can manifest themselves e.g. emergent relationships that differ from CMIP3 to CMIP5 (Caldwell et al. 2018). The strong emergent relationships across the PPE with a single systematic error suggest parameter-related processes are the underlying reason and the difference in the two periods used for time-averaging suggest the early period variable is a predictor but also likely causal

in our climate model. The explanation of the mechanism in Sect. 4 supports this causality in our climate model.

We applied the “post-prediction” method to additional PPE experiments, newly identifying the drivers and calculating the regression coefficients, and attained similarly good correlation between the predicted (modelled) and actual AMOC strengths. The additional experiments were the non-flux-adjusted coupled PPE experiment (noFA-COUPLED) (the regions to average over to calculate the predictors were the same as that used for the main coupled PPE but the heat and freshwater fluxes used to calculate the predictors and the AMOC strength from the later years of the experiment used as the predictand were taken from noFA-COUPLED PPE) and the ATMOS experiment (using Arctic surface air temperature, Amazon and Orinoco runoffs and Tropical North Atlantic precipitation minus evaporation from the ATMOS PPE as predictors and the final 20-year average AMOC strength of the flux-adjusted coupled PPE focussed in the current study as the predictand).

We foresee two cases where our method could be applied or the qualitative results could be beneficial: building a coupled PPE, and developing a single coupled model. For this prediction to be used in practice, we need to define a way to discern a weakening member from a non-weakening member with a view to discontinuing the former. Figure 4 shows that for different thresholds we would make different amounts of false rejections and false inclusions. The choice of the threshold based on observations would be suitable for a single model. For building a PPE, it would depend on any systematic bias in AMOC strength; if a large fraction of PPE members are weak relative to the observed range, then a lower yet plausible threshold could be set to avoid rejecting a large number of parameter combinations.

The prediction method developed in the current study requires as input the AMOC transport data at the end of coupled spinup phase, so they are not useful as a warning by themselves. We were able to make the prediction only because we had a PPE to train the statistical model. In practice, PPEs with other coupled models will need to at least run 20 coupled spinups to identify the key drivers and train up their own statistical model. PPEs based on different models might identify drivers that are different from the four we see here. But it only uses the spinup phase of the entire experiment, and it could save huge amounts of wasted computer runs, especially when building a coupled PPE. So for modellers that run coupled PPEs, this method is a valuable approach for not wasting resources on members where the AMOC will weaken too much. Different PPEs might expose new drivers and it would be worth the PPE community pooling these.

For developing a single model, developers would need to also run a PPE of spinups to use the statistical prediction. For model developers who do not currently use PPEs, we

suggest that PPEs are a valuable addition to their toolkit and the methods outlined here could add valuable insight into the key mechanisms driving the behaviour of the AMOC in their own model. However, for model developers who do not have a PPE and will not build a PPE, we suggest that there is still value in evaluating our drivers or a pooled set of drivers in the spinups of their climate model and other CMIP climate models to help them qualitatively understand the strength of their AMOC.

We suggest that there is value in evaluating our drivers because the mechanisms may be relevant to other models as well. Three of the key drivers identified in this study are known to be individually important to the AMOC strength, either because they affect density in the SPG region directly or by the affected water overflowing into the SPG region. Many studies have shown the importance of density in the SPG to AMOC strength (Ortega et al. 2021; Lin et al. 2023) so a cooling would be expected to increase the AMOC strength, even though (as shown in this study), advective feedbacks can then lead to the SPG to become warmer and saltier (but still denser). Also, Sévellec et al. (2017) found that freshening from the loss of Arctic sea ice caused the AMOC to weaken (though increased heat uptake caused most of the weakening), and Jahfer et al. (2020) conducted sensitivity experiments with no and doubled Amazon runoff and found the AMOC to strengthen and weaken, respectively. Future research to understand the importance of these drivers in other climate models may help to reduce biases and uncertainty in the modelling of the AMOC (Jackson et al. 2023).

In this study, in our search for drivers of the AMOC strength, we primarily focussed on the ocean fluxes and not on atmospheric variables (except for those related to SPG cooling referred to in Sect. 4.1). This is because we view the problem directly from the viewpoint of the physical mechanisms in the ocean model via its governing equations for ocean tracers and circulation. Whatever atmospheric influences there may be (and there will doubtlessly be because the changes in the AMOC strength arise as the result of parameter perturbations to the atmosphere and land models), they will inevitably enter the ocean model equations in the form of fluxes exchanged through the air-sea interface. It is these fluxes that we examine in this study and use to predict the AMOC strength. Furthermore, if an atmosphere variable is identified as a driver of the AMOC strength, a physical mechanism linking the atmospheric variable and the AMOC strength would need to be elucidated. This necessitates identifying an intermediary step in the form of ocean fluxes. Therefore, it is imperative to identify ocean drivers of the AMOC strength first. This is the justification for prioritising the search for oceanic drivers.

Many studies have predicted that the AMOC will weaken under global warming (e.g. Collins et al. 2013; Jackson et al.

2020). An implication of this study is that, in particular, SPG warming and Arctic freshening may pose a large impact. Another is that a fresher tropical North Atlantic from river outflow may be another cause of the AMOC slowdown.

Supplementary Information The online version contains supplementary material available at <https://doi.org/10.1007/s00382-024-07159-5>.

Acknowledgements We thank the three anonymous reviewers for their insightful and constructive comments. We are grateful to John Rostron, Carol McSweeney, James Murphy and Glen Harris for their contributions in the production of UKCP18 PPE data.

Funding The authors were supported by the Met Office Hadley Centre Climate Programme funded by DSIT.

Data availability The datasets generated during and/or analysed during the current study are available in the GitHub repository, https://github.com/qump-project/qump-hadgem3/tree/master/data/AMOC_paper

Declarations

Conflict of interest The authors have no relevant financial or non-financial interests to disclose.

Open Access This article is licensed under a Creative Commons Attribution 4.0 International License, which permits use, sharing, adaptation, distribution and reproduction in any medium or format, as long as you give appropriate credit to the original author(s) and the source, provide a link to the Creative Commons licence, and indicate if changes were made. The images or other third party material in this article are included in the article's Creative Commons licence, unless indicated otherwise in a credit line to the material. If material is not included in the article's Creative Commons licence and your intended use is not permitted by statutory regulation or exceeds the permitted use, you will need to obtain permission directly from the copyright holder. To view a copy of this licence, visit <http://creativecommons.org/licenses/by/4.0/>.

References

- Best MJ, Pryor M, Clark DB, Rooney GG, Essery RLH, Ménard CB, Edwards JM, Hendry MA, Gedney N, Mercado LM, Sitch S, Blyth E, Boucher O, Cox PM, Grimmond CSB, Harding RJ (2011) The Joint UK Land Environment Simulator (JULES), model description—Part 1: Energy and water fluxes. *Geosci Model Dev* 4:677–699. <https://doi.org/10.5194/gmd-4-677-2011>
- Caldwell PM, Zelinka MD, Klein SA (2018) Evaluating emergent constraints on equilibrium climate sensitivity. *J Clim* 31(10):3921–3942. <https://doi.org/10.1175/JCLI-D-17-0631.1>
- CICE Consortium, 2017, CICE Documentation, Madec <https://cice-consortium-cice.readthedocs.io/en/cice6.0.0.alpha/index.html>
- Clark DB, Mercado LM, Sitch S, Jones CD, Gedney N, Best MJ, Pryor M, Rooney GG, Essery RLH, Blyth E, Boucher O, Cox PM, Harding RJ (2011) The joint UK land environment simulator (JULES), model description—Part 2: Carbon fluxes and vegetation. *Geosci Model Dev* 4:701–722. <https://doi.org/10.5194/gmd-4-701-2011>
- Collins M, Knutti R, Arblaster J, Dufresne J-L, Fichefet R, Friedlingstein P, Gao X, Gutowski WJ, Johns T, Krinner G, Shongwe M, Tebaldi C, Weaver AJ, Wehner M (2013) Long-term Climate Change: Projections, Commitments and Irreversibility. In: *Climate Change 2013: The Physical Science Basis. Contribution of Working Group I to the Fifth Assessment Report of the Intergovernmental Panel on Climate Change* [Stocker, T.F., D. Qin, G.-K. Plattner, M. Tignor, S.K. Allen, J. Boschung, A. Nauels, Y. Xia, V. Bex and P.M. Midgley (eds.)]. Cambridge University Press, Cambridge, United Kingdom and New York, NY, USA.
- Hewitt HT, Copeley D, Culverwel ID, Harris CM, Hill RSR, Keen AB, McLaren AJ, Hunke EC (2011) Design and implementation of the infrastructure of HadGEM3: the next-generation met office climate modelling system. *Geosci Model Dev* 4:223–253. <https://doi.org/10.5194/gmd-4-223-2011>
- Hunke EC, Lipscomb WH (2008) CICE: the Los Alamos sea ice model documentation and software users manual, Version 4.0
- Ivanova DP, McClean JL, Hunke EC (2012) Interaction of ocean temperature advection, surface heat fluxes and sea ice in the marginal ice zone during the North Atlantic Oscillation in the 1990s: a modeling study. *J Geophys Res* 117:C02031. <https://doi.org/10.1029/2011JC007532>
- Jackson LC, Kahana R, Graham T, Ringer MA, Woollings T, Mecking JV, Wood RA (2015) Global and European climate impacts of a slowdown of the AMOC in a high resolution GCM. *Clim Dyn* 45:3299–3316. <https://doi.org/10.1007/s00382-015-2540-2>
- Jackson LC, Roberts MJ, Hewitt HT, Iovino D, Koenigk T, Meccia VL, Roberts CD, Ruprich-Robert Y, Wood RA (2020) Impact of ocean resolution and mean state on the rate of AMOC weakening. *Clim Dyn* 55:711–732. <https://doi.org/10.1007/s00382-020-05345-9>
- Jackson LC, Hewitt HT, Bruciaferri B, Calvert D, Graham T, Guiavarc'h C, Menary MB, New AL, Roberts M, Storkey D (2023) Challenges simulating the AMOC in climate models. *Phil Trans R Soc A381*:20220187. <https://doi.org/10.1098/rsta.2022.0187>
- Jahfer S, Vinayachandran PN, Nanjundiah RS (2020) The role of Amazon river runoff on the multidecadal variability of the Atlantic ITCZ. *Environ Res Lett* 15:054013. <https://doi.org/10.1088/1748-9326/ab7c8a>
- Karmalkar AV, Sexton DMH, Murphy JM, Booth BBB, Rostron JW, McNeill DJ (2019) Finding plausible and diverse variants of a climate model. Part II: development and validation of methodology. *Clim Dyn* 53:1–31. <https://doi.org/10.1007/s00382-019-04617-3>
- Lee LA, Pringle KJ, Reddington CL, Mann GW, Stier P, Spracklen DV, Pierce JR, Carslaw KS (2013) The magnitude and causes of uncertainty in global model simulations of cloud condensation nuclei. *Atmos Chem Phys* 13:8879–8914. <https://doi.org/10.5194/acp013-8879-2013>
- Lin Y-J, Rose BEJ, Hwang Y-T (2023) Mean state AMOC affects AMOC weakening through subsurface warming in the Labrador Sea. *J Clim* 36(12):3895–3915. <https://doi.org/10.1175/JCLI-D-22-0464.1>
- Madec G, Bourdallé-Badie R, Bouttier P-A, Bricaud C, Bruciaferri D, Calvert D, Chanut J, Clementi E, Coward A, Delrosso D, Ethé C, Flavoni S, Graham T, Harle J, Iovino D, Lea D, Lévy C, Lovato T, Martin N, Masson S, Mocavero S, Paul J, Rousset C, Storkey D, Storto A, Vancoppenolle M (2017) NEMO ocean engine. In: *Notes du Pôle de modélisation de l'Institut Pierre-Simon Laplace (IPSL) (v3.6-patch, Number 27)*. Zenodo. <https://doi.org/10.5281/zenodo.3248739>
- Menary MB, Roberts CD, Palmer MD, Halloran PR, Jackson L, Wood RA, Müller WA, Matei D, Lee S (2013) Mechanisms of aerosol-forced AMOC variability in a state of the art climate model. *J Geophys Res Ocean* 118(4):2087–2096. <https://doi.org/10.1002/jgrc.20178>
- Moat BI, Frajka-Williams E, Smeed D, Rayner D, Johns WE, Baringer MO, Volkov DL, Collins J (2022) Atlantic meridional overturning circulation observed by the RAPID-MOCHA-WBTS (RAPID-Meridional Overturning Circulation and Heatflux Array-Western Boundary Time Series) array at 26N from 2004 to 2020 (v2020.2).

- NERC EDS British Oceanographic Data Centre NOC. <https://doi.org/10.5285/e91b10af-6f0a-7fa7-e053-6c86abc05a09>
- Murphy JM, Sexton DMH, Barnett DN, Jones G, Webb MJ, Collins M, Stainforth DA (2004) Quantification of modelling uncertainties in a large ensemble of climate change simulations. *Nature* 430:768–772. <https://doi.org/10.1038/nature02771>
- Murphy JM, Harris GR, Sexton DMH, Kendon EJ, Bett PE, Clark RT, Eagle KE, Fosse G, Fung F, Lowe J A, McDonald RE, McInnes RN, McSweeney CF, Mitchell JFB, Rostron JW, Thornton HE, Tucker S, Yamazaki K (2018) UKCP18 land projections: science report. <https://www.metoffice.gov.uk/pub/data/weather/uk/ukcp18/science-reports/UKCP18-Land-report.pdf>
- Oki T, Sud YC (1998) Design of Total Runoff Integrating Pathways (TRIP)—A global river channel network. *Earth Interact* 2:1–36. [https://doi.org/10.1175/1087-3562\(1998\)002%3c0001:DOTRIP%3e2.3.CO;2](https://doi.org/10.1175/1087-3562(1998)002%3c0001:DOTRIP%3e2.3.CO;2)
- Ortega P, Robson JI, Menary M, Sutton RT, Blaker A, Germe A, Hirschi JJ-M, Sinha B, Hermanson L, Yeager S (2021) Labrador Sea subsurface density as a precursor of multidecadal variability in the North Atlantic: a multi-model study. *ESD* 12(2):419–438. <https://doi.org/10.5194/esd-12-419-2021>
- Robson J, Hodson D, Hawkins E (2014) Atlantic overturning in decline? *Nature Geosci* 7:2–3. <https://doi.org/10.1038/ngeo2050>
- Rostron JW, Sexton DMH, McSweeney CF, Yamazaki K, Andrews T, Furtado K, Ringer MA, Tsushima Y (2020) The impact of performance filtering on climate feedbacks in a perturbed parameter ensemble. *Clim Dyn* 55:521–551. <https://doi.org/10.1007/s00382-020-05281-8>
- Rowlands DJ, Frame DJ, Ackerley D, Aina T, Booth BBB, Christensen C, Collins M, Faull N, Forest CE, Grandey BS, Gryspeerd E, Highwood EJ, Ingram WJ, Knight S, Lopez A, Massey N, McNamara F, Meinshausen N, Piani C, Rosier SM, Sanderson BM, Smith LA, Stone DA, Thurston M, Yamazaki K, Yamazaki YH, Allen MR (2012) Broad range of 2050 warming from an observationally constrained large climate model ensemble. *Nature Geosci* 5:256–260. <https://doi.org/10.1038/ngeo1430>
- Sanderson BM (2011) A multimodel study of parametric uncertainty in predictions of climate response to rising greenhouse gas concentrations. *J Clim* 24(5):1362–1377. <https://doi.org/10.1175/2010JCLI3498.1>
- Sévellec F, Fedorov A, Liu W (2017) Arctic sea-ice decline weakens the Atlantic meridional overturning circulation. *Nature Clim Change* 7:604–610. <https://doi.org/10.1038/nclimate3353>
- Sexton DMH, McSweeney CF, Rostron JW, Yamazaki K, Booth BBB, Murphy JM, Regayre L, Johnson JS, Karmalkar AV (2021) A perturbed parameter ensemble of HadGEM3-GC3.05 coupled model projections: part 1: selecting the parameter combinations. *Clim Dyn* 56:3395–3436. <https://doi.org/10.1007/s00382-021-05709-9>
- Sexton D, Yamazaki K, Murphy J, Rostron J (2020) Assessment of drifts and internal variability in UKCP projections. <https://www.metoffice.gov.uk/binaries/content/assets/metofficegovuk/pdf/research/ukcp-climate-drifts-report.pdf>
- Shiogama H, Watanabe M, Yoshimori M, Yokohata T, Ogura T, Annan J D, Hargreaves J C, Abe M, Kamae Y, O'ishi R, Nobui R, Emori S, Nozawa T, Abe-Ouchi A, Kimoto M (2012) Perturbed physics ensemble using the MIROC5 coupled atmosphere–ocean GCM without flux corrections: Experimental design and results. *Clim Dyn* 39, 3041–3056. <https://doi.org/10.1007/s00382-012-1441-x>
- Stainforth DA et al (2005) Uncertainty in predictions of the climate response to rising levels of greenhouse gases. *Nature* 433:403–406. <https://doi.org/10.1038/nature03301>
- Thorpe RB, Gregory JM, Johns TC, Wood RA, Mitchell JFB (2001) Mechanisms determining the Atlantic thermohaline circulation response to greenhouse gas forcing in a non-flux-adjusted coupled climate model. *J Clim* 14(14):3102–3116. [https://doi.org/10.1175/1520-0442\(2001\)014%3c3102:MDTATC%3e2.0.CO;2](https://doi.org/10.1175/1520-0442(2001)014%3c3102:MDTATC%3e2.0.CO;2)
- Vellinga M, Wu P (2004) Low-latitude freshwater influence on centennial variability of the Atlantic thermohaline circulation. *J Clim* 17:4498–4511. <https://doi.org/10.1175/3219.1>
- Walters D, Baran AJ, Boutle I, Brooks M, Earnshaw P, Edwards J, Furtado K, Hill P, Lock A, Mannes J, Morcrette C, Mulcahy J, Sanchez C, Smith C, Stratton R, Tennant W, Tomassini L, Van Weverberg K, Vosper S, Willett M, Browse J, Bushell A, Carslaw K, Dalvi M, Essery R, Gedney N, Hardiman S, Johnson B, Johnson C, Jones A, Jones C, Mann G, Milton S, Rumbold H, Sellar A, Ujjié M, Whital, M, Williams K, Zerroukat M (2019) The Met Office Unified Model Global Atmosphere 7.0/7.1 and JULES Global Land 7.0 configurations. *Geosci Model Dev*, 1909–1963. 10.5194/gmd-12-1909-2019
- Williams KD, Copsey D, Blockley EW, Bodas-Salcedo A, Calvert D, Comer R, Davis P, Graham T, Hewitt HT, Hill R, Hyder P, Ineson S, Johns TC, Keen AB, Lee RW, Megann A, Milton SF, Rae JGL, Roberts MJ, Scaife AA, Schiemann R, Storkey D, Thorpe L, Watterson IG, Walters DN, West A, Wood RA, Woollings T, Xavier PK (2018) The Met Office Global Coupled Model 3.0 and 3.1 (GC3.0 and GC3.1) Configurations. *JAMES*, 10, 2, 357–380. <https://doi.org/10.1002/2017MS001115>
- Yamazaki K, Sexton DMH, Rostron JW, McSweeney CF, Murphy JM, Harris GR (2021) A perturbed parameter ensemble of HadGEM3-GC3.05 coupled model projections: part 2: global performance and future changes. *Clim Dyn* 56:3437–3471. <https://doi.org/10.1007/s00382-020-05608-5>

Publisher's Note Springer Nature remains neutral with regard to jurisdictional claims in published maps and institutional affiliations.